Nuclear Physics B127 (1977) 365- 383

GENERAL FEATURES OF $\bar{p}p$ INTERACTIONS AT 32 GeV/c

M.A. JABIOL, J.P. LAUGIER and C. LOUEDEC
DPhPE., CEN-Saclay, France

C. DUJARDIN *, J. HANTON *, J. LAURENT and R. WINDMOLDERS
Faculté des Sciences, Université de l'Etat, Mons, Belgium

E.P. KISTENEV, A.A. MINAENKO, A.M. MOISEEV and E.A. STARCHENKO
IHEP, Serpukhov, USSR

E. DE WOLF [+]*, J.J. DUMONT * and M. GIJSEN *
Interuniversity Institute for High Energies, ULB-VUB, Brussels, Belgium

France-Soviet Union and CERN-Soviet Union Collaborations

Received 10 June 1977
(Revised 3 July 1977)

The general features of $\bar{p}p$ interactions at 32 GeV/c are analysed in a bubble chamber experiment with a statistics of 5.2 μb/event. The inclusive production of neutral strange particles and pions is analysed and compared to results obtained at other energies and in pp interactions. Total cross sections are determined for various 4C reactions and the relative contributions of diffractive dissociation and $\Delta\Delta$ production to the reaction $\bar{p}p \to \bar{p}p\pi^+\pi^-$ are estimated.

1. Introduction

We present here some general features of $\bar{p}p$ interactions at 32 GeV/c. The data are obtained from the analysis of about 12 000 pictures taken in the Mirabelle bubble chamber exposed to a RF separated beam at the Serpukhov accelerator. The pictures were scanned twice for all interactions in a 2 m long fiducial volume with an overall efficiency of 99%. The events were measured on film plane digitizers and reconstructed with the Hydra geometry. 4C fits were attempted for all

* IISN–IIKW, Belgium.
[+] Also at Universitaire Instelling, Antwerp, Belgium.

topologies using either Grind or Hydra kinematics. Finally all reconstructed events were checked on the scanning table in order to flag slow protons ($P_{lab} < 1.2$ GeV/c), and to discard fits inconsistent with the observed bubble densities. After two passes the overall efficiency for data processing is of the order of 85%.

In the following sections we will successively evaluate the topological cross sections, analyse the inclusive production of neutral particles and of charged pions and analyse the 4-constraint reactions.

2. Topological cross sections

The sample used in this analysis includes 5726 events and corresponds to 5.2 μb/event. Topological cross sections are obtained by normalizing the total number of events corrected for scanning and processing losses to the total cross section of 46 mb [1]. Elastic events were selected on the basis of the kinematical fits and corrections were applied to take into account the events which failed to give a 4C fit (~5% of the total elastic sample) and the unobservable events near the forward direction ($|t| < 0.06$ GeV^2). The resulting elastic cross section

Table 1
Topological cross sections

Topology	$\sigma_{\bar{p}p}$(mb)	$\sigma_{\bar{p}p}$(mb) P_{lab} (proton) < 1.2 (GeV/c)	σ_{pp}(mb)	$\sigma_{\bar{p}p} - \sigma_{pp}$(mb)
0	0.46 ± 0.06			0.46 ± 0.06
2	15.96 ± 0.30		15.4 ± 0.4	0.56 ± 0.42
2 el	8.68 ± 0.24		8.33 ± 0.3	
2 inel	7.28 ± 0.23	2.85 ± 0.14	7.06 ± 0.3	$0.22 \pm \begin{matrix}0.4\\0.2\end{matrix}$
4	12.23 ± 0.29	4.59 ± 0.18	11.2 ± 0.3	1.03 ± 0.42
6	9.58 ± 0.26	2.09 ± 0.13	7.4 ± 0.3	2.18 ± 0.36
8	4.92 ± 0.19	0.47 ± 0.06	3.2 ± 0.2	1.72 ± 0.28
10	2.16 ± 0.12	0.06 ± 0.02	0.98 ± 0.1	1.15 ± 0.17
12	0.52 ± 0.06		0.13 ± 0.05	0.39 ± 0.08
14	0.14 ± 0.03		0.09 ± 0.03	0.05 ± 0.04
16	0.02 ± 0.01			0.02 ± 0.015
Total inel.	37.31 ± 0.51	9.98 ± 0.4	30.1 ± 0.6	7.23 ± 0.8
Total	45.99 ± 0.60		38.4 ± 0.6	
	$\langle n_c \rangle = 5.09 \pm 0.03$ $D = (\langle n_c^2 \rangle - \langle n_c \rangle^2)^{1/2}$ $= 2.54 \pm 0.8$ $f_2 = \langle n_c(n_c - 1) \rangle / \langle n_c \rangle^2$ $= 1.29 \pm 0.15$	$\langle n_p \rangle = 0.27 \pm 0.03$		$\langle n_c \rangle = 6.7 \pm 0.7$ $D = 3.0 \pm 1.0$

(8.7 ± 0.3 mb) is in agreement with the value given in ref. [2] (8.8 ± 0.5 mb). A correction has also been applied for the loss of inelastic 2-prong events with $|t| < 0.03$ GeV^2. The corrected topological cross sections and the cross sections for events with an identified proton are listed in table 1. Preliminary values of these cross sections which are in agreement with the present values have already been published [3,4]. The average charged multiplicity $\langle n_c \rangle$ per inelastic event is found equal to 5.09 ± 0.03 and the average number of recognized protons $\langle n_p \rangle$ per inelastic event is equal to 0.27 ± 0.03. A comparison with the interpolated pp topological cross sections [5] shows that the annihilation cross sections $\sigma_{\bar{p}p}^{(n)} - \sigma_{pp}^{(n)}$ are on average associated to a higher multiplicity:

$$\langle n_c \rangle^{annih} = 6.7 \pm 0.7 .$$

3. Inclusive particle production

3.1. V^0 events

3.1.1. Total cross sections and multiplicities

A total of 1268 V^0's fitting either the γ, the K^n (K^0 or $\bar{K}^0$), the Λ or the $\bar{\Lambda}$ hypothesis were found in the present analysis. The V^0's ambiguous between an e^+e^- pair and a hadronic hypothesis (<1% of the total) were assigned to the e^+e^- channel. Those fitting several hadronic hypotheses (~4% of the total) were removed from the sample and the remaining ones were weighted by a momentum-dependent factor taking into account the probability to yield an unambiguous fit. The usual corrections for decays (or γ conversion) outside the fiducial volume or too close to the production vertex and for unseen decay modes were also applied. The resulting cross sections are listed in table 2.

The values of σ_Λ and $\sigma_{\bar{\Lambda}}$ are compatible within errors as required by C invariance. The inclusive π^0 cross section (assumed to be half of the γ cross section), the K^n and the combined $\Lambda/\bar{\Lambda}$ cross sections are shown in fig. 1 together with values

Table 2
Total inclusive cross sections corrected for unseen decays and average multiplicities for γ, K^n, Λ and $\bar{\Lambda}$ production

	Number of observed unambiguous V^0's	σ(mb)	$\langle n \rangle$
γ	940	140.0 ± 4.3	3.75 ± 0.12
K^n	156	6.2 ± 0.7	0.17 ± 0.02
Λ	79	1.8 ± 0.3	0.048 ± 0.005
$\bar{\Lambda}$	51	1.4 ± 0.3	0.037 ± 0.005

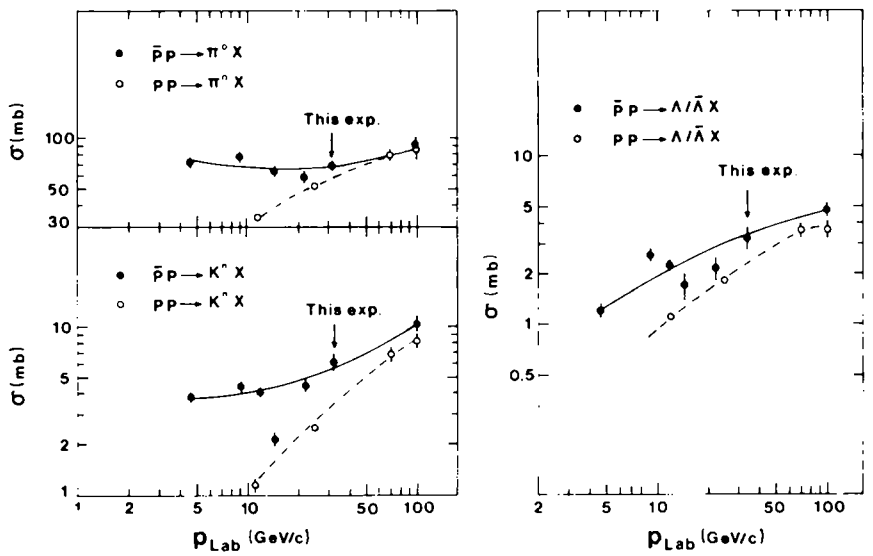

Fig. 1. Inclusive cross sections for π^0, K^n and $\Lambda/\bar{\Lambda}$ production in $\bar{p}p$ and pp interactions as a function of P_{lab}. The curves are only to guide the eye.

obtained at other energies and in pp interactions [6,7]. We observe that our results fit rather well with the 12, 22 and 100 GeV/c data. The three cross sections clearly increase at a slower rate than in pp interactions in the same energy range.

The topological cross sections for π^0, K^n and $\Lambda/\bar{\Lambda}$ production are listed in table 3. In order to compare these values with data at different energies we present in fig. 2 the dependence of the average number of π^0's, K^n's and $\Lambda/\bar{\Lambda}$'s on the number of charged particles and in fig. 3 the fractions of the inclusive K^n and $\Lambda/\bar{\Lambda}$ cross sections corresponding to each topology. Although the statistical errors are large

Table 3
Topological cross sections for π^0, K^n and $\Lambda/\bar{\Lambda}$ production

Number of prongs	σ_{π^0}(mb)	σ_{K^n}(mb)	$\sigma_{\Lambda/\bar{\Lambda}}$(mb)
0	0.96 ± 0.19	0.19 ± 0.10	0.057 ± 0.03
2	10.22 ± 0.86	1.00 ± 0.19	0.87 ± 0.15
4	20.06 ± 1.20	1.59 ± 0.24	1.14 ± 0.17
6	22.55 ± 1.36	1.86 ± 0.27	0.86 ± 0.14
8	10.59 ± 0.83	0.96 ± 0.19	0.17 ± 0.06
10	4.43 ± 0.60	0.35 ± 0.13	0.026 ± 0.026
12	1.00 ± 0.32	0.25 ± 0.18	
14	0.10 ± 0.07		
16	0.10 ± 0.05		

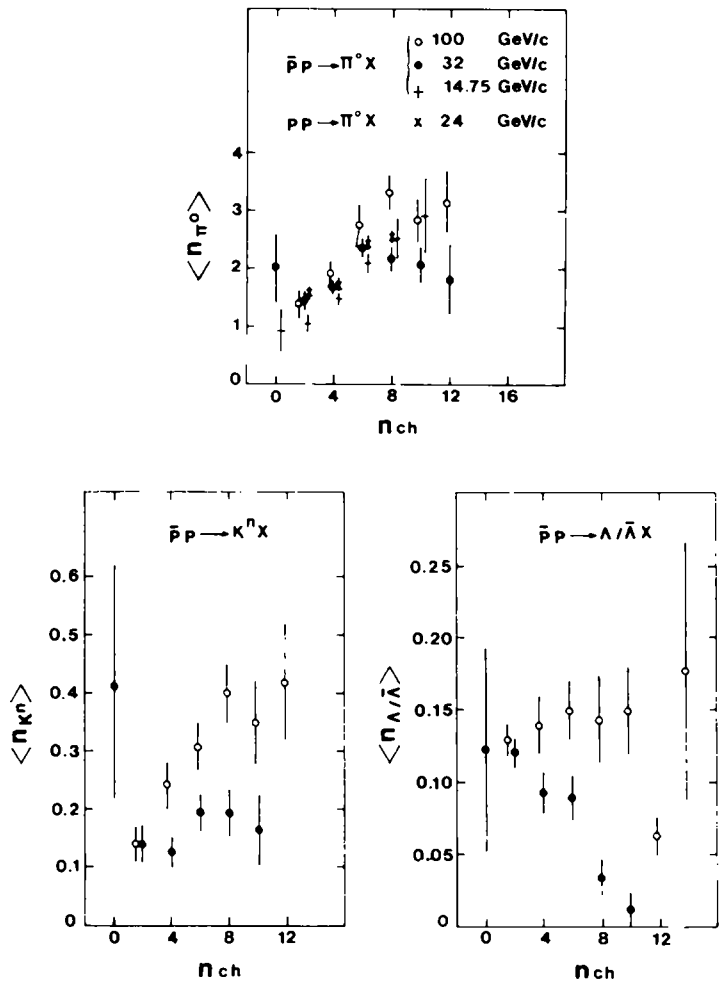

Fig. 2. Average π^0, K^n and $\Lambda/\bar{\Lambda}$ multiplicities as a function of the charged multiplicities for $\bar{p}p$ interactions.

we observe that the dependence of $\langle n_{K^n} \rangle$ on the number of charged prongs is weaker at 32 than at 100 GeV/c. A strong difference also appears in the behaviour of $\langle n_{\Lambda/\bar{\Lambda}} \rangle$ which is almost independent of the topology at 100 GeV/c and strongly decreasing at 32 GeV/c. Furthermore it is interesting to note that at the two energies considered in fig. 3, K^n production is on average associated to a higher charge multiplicity than $\Lambda/\bar{\Lambda}$ production.

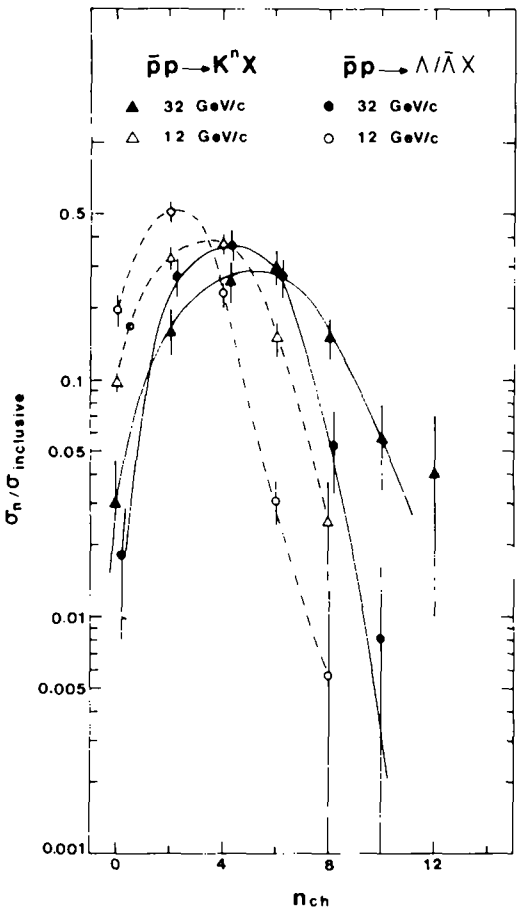

Fig. 3. Ratio of the K^n and $\Lambda/\bar{\Lambda}$ inclusive cross sections for a given charged multiplicity to the total inclusive cross sections. The curves are drawn to guide the eye.

3.1.2. Differential cross sections

The invariant structure functions

$$F(x) = \frac{2}{\pi\sqrt{s}} \int E^* \cdot \frac{d^2\sigma}{dx\,dp_T^2}\, dp_T^2 \ ,$$

where $x = (p_\parallel^*/p^{*\max})$ are shown in figs. 4 a c for γ, K^n, Λ and $\bar{\Lambda}$ production respectively. The first two distributions (which are expected to be symmetric by C invariance) have been folded around $x = 0$. The third one shows that Λ's and $\bar{\Lambda}$'s are preferentially emitted in the backward and forward hemispheres respectively. The combined $\Lambda/\bar{\Lambda}$ distribution folded around $x = 0$ is shown in fig. 4d.

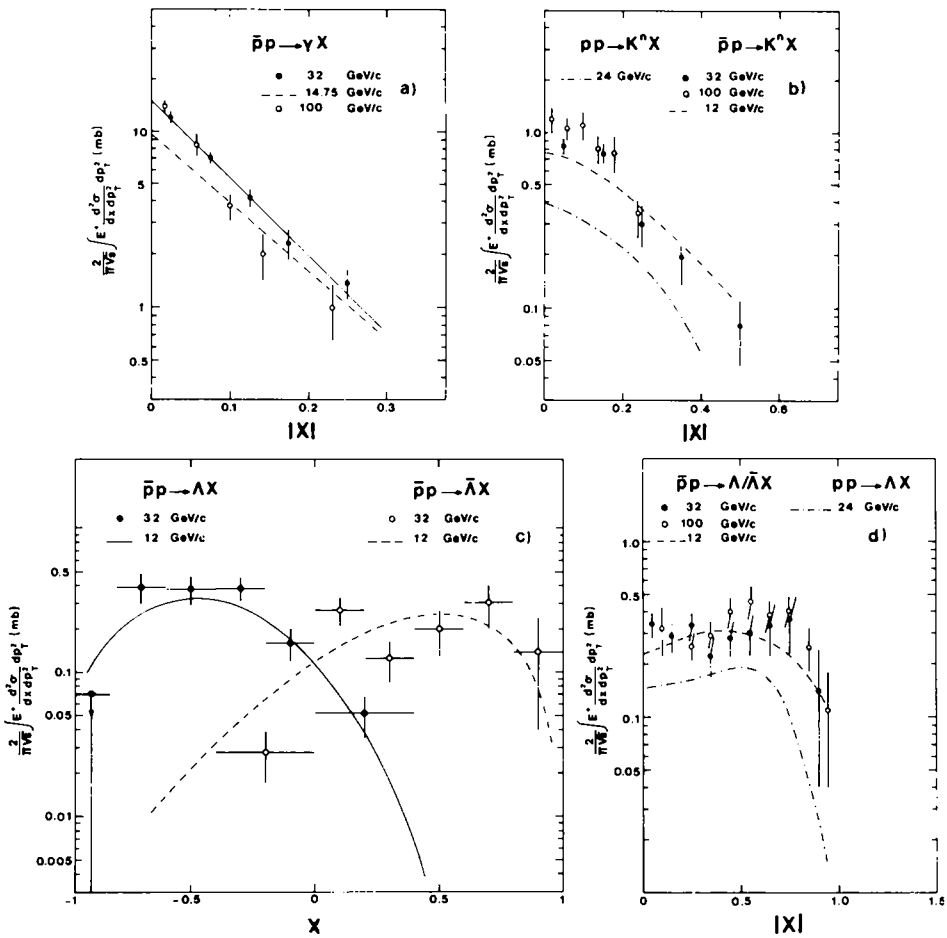

Fig. 4. The invariant structure function $F(x)$ for γ, K^n, Λ and $\bar{\Lambda}$ production. The full line on (a) shows the result of the fit to an exponential distribution.

Table 4
Average transverse momentum for γ, K_n and $\Lambda/\bar{\Lambda}$ production at 32 and 100 GeV/c

$\langle P_T \rangle$ (GeV/c)		
P_{lab}	32 GeV/c	100 GeV/c
γ	0.17 ± 0.01	0.16 ± 0.01
K_n	0.43 ± 0.05	0.46 ± 0.03
$\Lambda/\bar{\Lambda}$	0.45 ± 0.05	0.52 ± 0.04

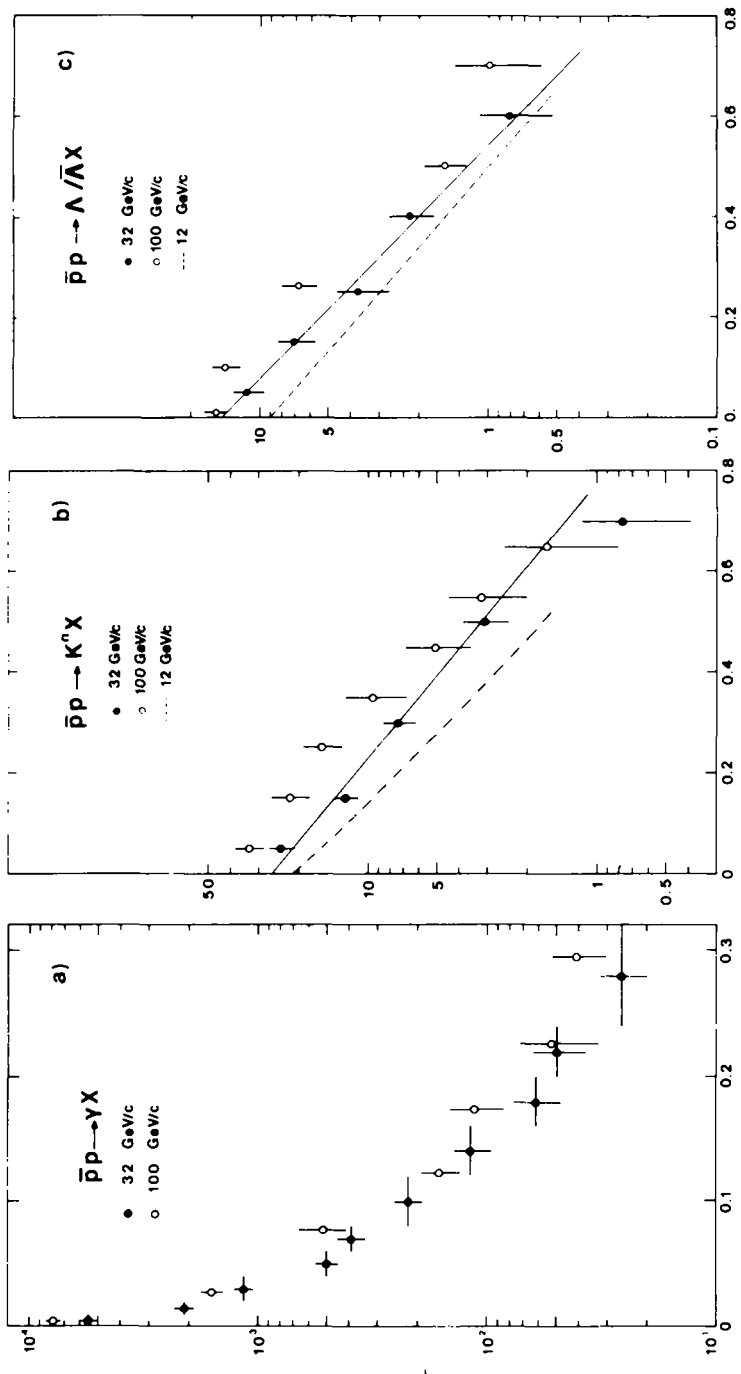

Fig. 5. Distributions of the transverse momentum squared for γ, K^0 and $\Lambda/\bar{\Lambda}$ production. The full lines show the results of fits to exponential distributions.

For γ production we observe that the structure function peaks at $|x| = 0$ and can be described by an exponential $Ae^{-B|x|}$ with $B = 10.7 \pm 0.7$. A similar behaviour has been observed at 14.75 and 100 GeV/c [6c, 8a] but the distributions seem to become slightly steeper with increasing energy. Furthermore for $0.05 < |x| < 0.25$ our results seem to fall slightly above the 100 GeV/c data.

The structure functions for K^n and $\Lambda/\bar{\Lambda}$ production show little energy dependence between 12 and 100 GeV/c. On the other hand, the corresponding structure functions for pp interactions at 24 GeV/c [7a] are systematically lower than those for $\bar{p}p$ interactions by a factor of ~2 over the whole range of x.

The average values of the transverse momentum for γ's, K^n's and $\Lambda/\bar{\Lambda}$'s are given in table 4. They are very close to the values obtained at 100 GeV/c. The same similarity appears in the p_T^2 distributions (fig. 5) which seem to be almost energy-independent except for an overall normalization factor. Fits to exponential distribu-

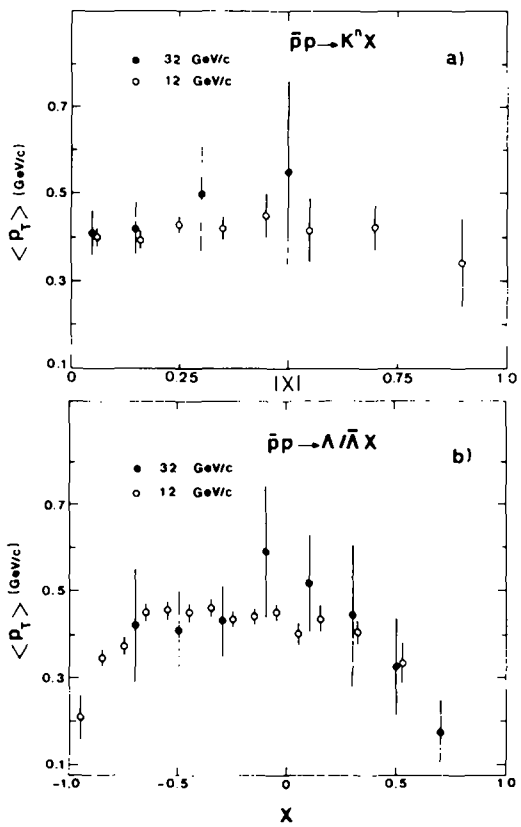

Fig. 6. Average values of the transverse momentum in different intervals of x for K^n and $\Lambda/\bar{\Lambda}$ production.

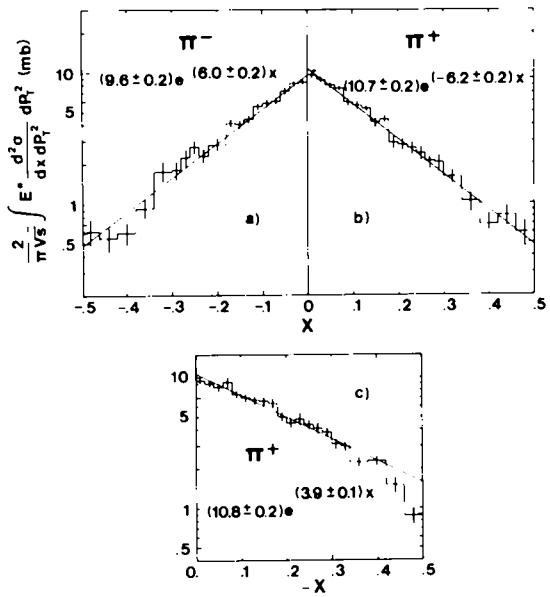

Fig. 7. The invariant structure function $F(x)$ for negative pions in the backward hemisphere (a) and for positive pions in the forward (b) and backward (c) hemispheres.

tions yield the following values of the slopes:

$b = 4.2 \pm 0.8\ (\mathrm{GeV}/c)^{-2}$ for K^{n} ,

$b = 5.0 \pm 0.9\ (\mathrm{GeV}/c)^{-2}$ for $\Lambda/\bar{\Lambda}$.

Finally we show the average values of p_{T} for different intervals of x in fig. 6. The results are consistent with those obtained at 12 GeV/c.

3.2. $\pi^{\pm}$ production

In fig. 7 we show the invariant structure function $F(x)$ for all positive tracks considered as pions, except those otherwise identified by their bubble density or the results of the kinematical fit. This distribution is thus contaminated by unidentified protons and positive kaons. The same distribution is also given for negative pions produced in the backward hemisphere only, the forward one being too contaminated by unidentified antiprotons.

Fits to exponential distributions $A_{\pm}e^{b_{\pm}x}$ yield the following results:

$A_{-} = 9.6 \pm 0.2$ mb , $b_{-} = 6.0 \pm 0.2$, $(x < 0)$,

$A_{+} = 10.8 \pm 0.2$ mb , $b_{+} = 3.9 \pm 0.1$, $(x < 0)$,

$A_{+} = 10.7 \pm 0.2$ mb , $b_{+} = -6.2 \pm 0.2$, $(x > 0)$.

In the absence of any contamination the distributions for positive pions in the forward hemisphere and for negative pions in the backward hemisphere should be the same from C invariance. The results of the fits show that the slopes are indeed the same, but the normalizations differ by ~10%.

This effect is easily understood if one remembers that heavier particles considered as pions are shifted towards higher values of x. We thus expect the contamination to be stronger in the π^+ distribution than in the π^- distribution near $x = 0$.

The corresponding rapidity distributions $d\sigma/dy^*$ are shown in fig. 8. The proton contribution to the π^+ central region distribution ($-1.45 < y^* < 0.05$) has been removed by extrapolating the p_T^2 distribution of recognized protons taken as pions in each rapidity interval. On the other hand the K^+ contamination has been evaluated from the K^0 rapidity distribution assuming equal charged and neutral kaon production. The total correction amounts to ~20% at $y^* \approx 0$.

As stated previously the backward π^- distribution is expected to be almost un-

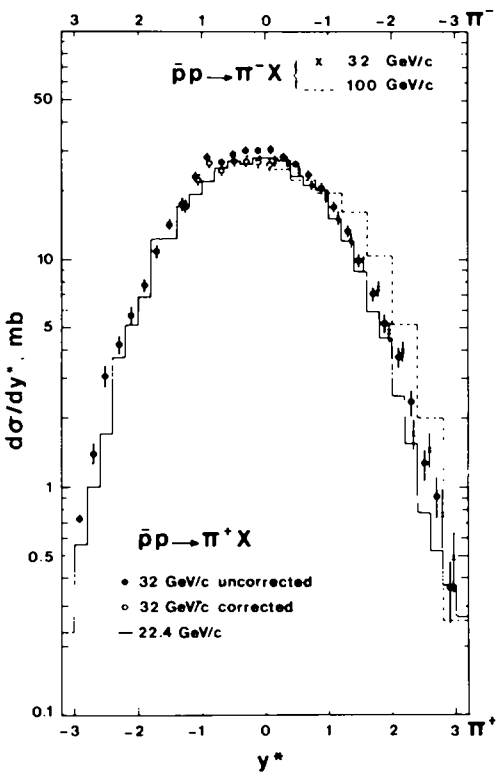

Fig. 8. Distribution of the π^+ rapidity in center of mass, considering all unidentified positive tracks as pions (•) and same distribution corrected for unidentified protons and K^+ (○); same distribution for π^- in the backward hemisphere (folded).

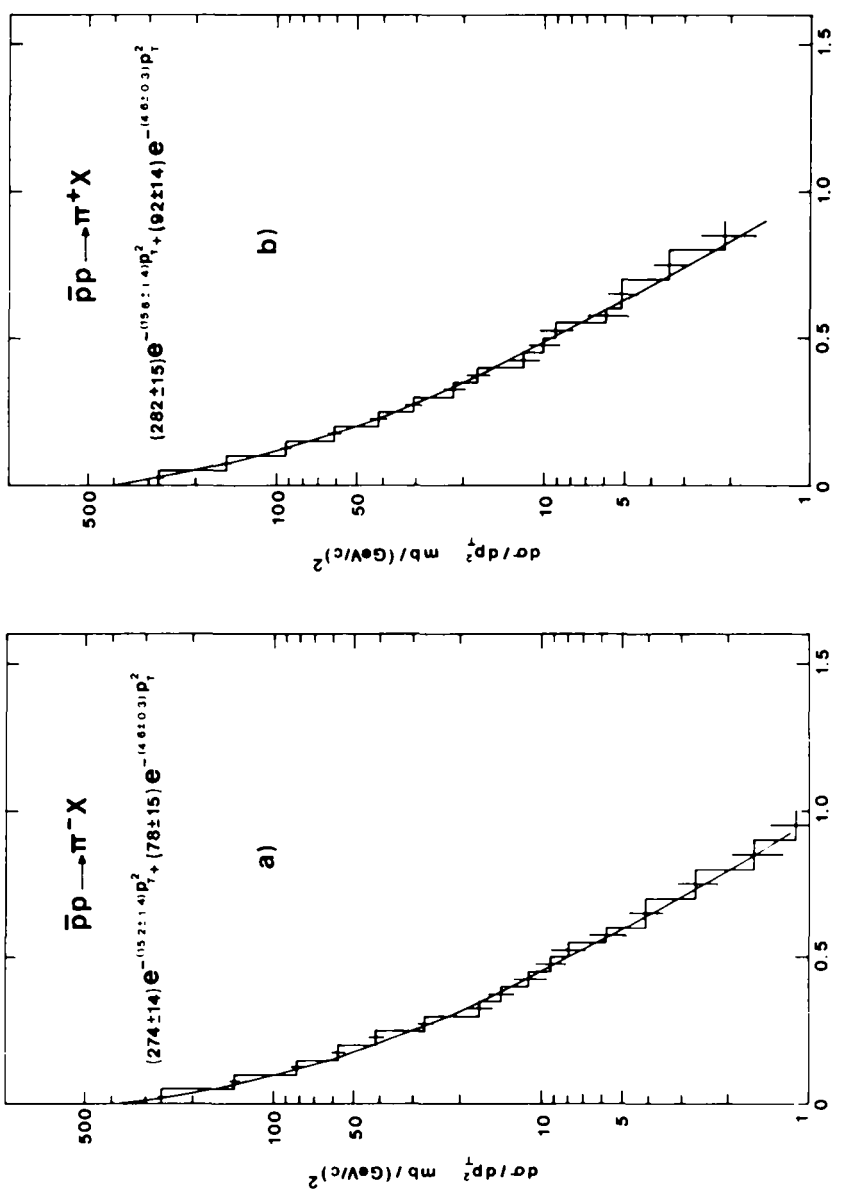

Fig. 9. Distribution of the transverse momentum squared for negative (positive) pions produced in the backward (forward) hemisphere (uncorrected for proton and K^+ contamination).

contaminated. This distribution has been folded around $y^* = 0$ to allow an easy comparison with forward π^+ production. The two distributions are compatible as required by C invariance. However the π^- distribution is slightly lower near $y^* = 0$ and becomes very close to the corrected backward π^+ distribution. For comparison the forward π^+ distribution at 22.4 GeV/c [6e] and the backward π^- distribution at 100 GeV/c [8b] are also shown. The distributions become wider with increasing energy but reach similar values in the central region.

The distributions of the transverse momentum squared are quite similar for π^+ and π^- (fig. 9). They clearly differ from an exponential shape but can be fitted by a sum of two terms:

$$\alpha \exp(-\beta P_T^2) + \gamma \exp(-\delta P_T^2)$$

with

$$\beta_+ = 15.6 \pm 1.4\ (\mathrm{GeV}/c)^{-2}, \qquad \delta_+ = 4.6 \pm 0.3\ (\mathrm{GeV}/c)^{-2},$$

$$\beta_- = 15.2 \pm 1.4\ (\mathrm{GeV}/c)^{-2}, \qquad \delta_- = 4.6 \pm 0.3\ (\mathrm{GeV}/c)^{-2}.$$

The average values of p_T integrated over the x distribution are respectively equal to 0.330 ± 0.002 GeV/c and 0.322 ± 0.002 GeV/c for π^+ and π^-. We observe also a strong correlation between p_T and x (fig. 10) with a reduction of $\langle P_T \rangle$ for $|x| \approx 0$ corresponding to the so-called seagull effect.

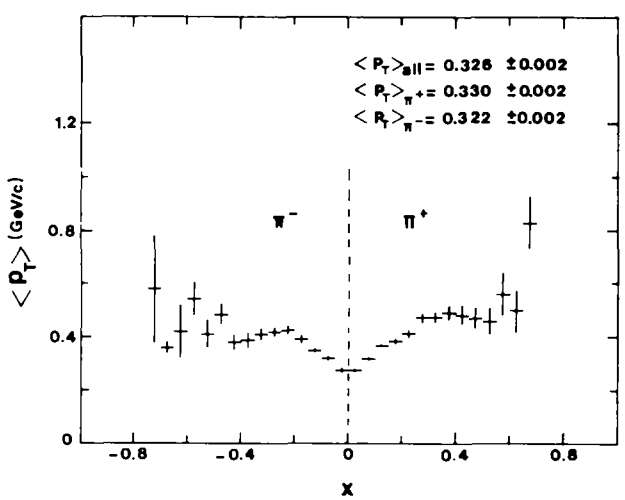

Fig. 10. Average values of the transverse momentum in different intervals of x for inclusive π^- production ($x < 0$) and π^+ production ($x > 0$)

4. Exclusive reactions

4.1. Total cross sections

The cross sections of the exclusive channels for which 4C fits were obtained are listed in table 5. 4C fits to annihilation channels are only obtained for the highest topologies (8 and 10 prongs). For all topologies the production of K^+K^- and $\bar{p}p$ pairs is very small compared to the production of $\pi^+\pi^-$ pairs. The production of multiple charged pion pairs is also reduced compared to the production of a single $\pi^+\pi^-$ pair. In order to check to what extend these effects depend on the incident energy and on the beam particle we show in fig. 11 the variation of the ratios

$$R_1 = \frac{\sigma(Ap \to Ap2\pi^+2\pi^-)}{\sigma(Ap \to Ap\pi^+\pi^-)}, \qquad R_2 = \frac{\sigma(Ap \to ApK^+K^-)}{\sigma(Ap \to Ap\pi^+\pi^-)},$$

$$A = \bar{p}, p, K^+, K^-, \pi^+, \pi^-,$$

with the Q value of the reaction [9,10]. Both R_1 and R_2 increase with the incident energy and seem to be more or less independent of the beam particle.

4.2. The reaction $\bar{p}p \to \bar{p}p\pi^+\pi^-$

As shown in table 5, this reaction is the most frequent 4C inelastic reaction and the only one for which an analysis can be performed with the present statistics (~200 events). The total cross section 1.34 ± 0.10 mb is in good agreement with

Table 5
Total cross sections for 4C reactions

Number of prongs	Reaction	σ(mb)
2	$\bar{p}p \to p\bar{p}$	8.67 ± 0.30
4	$\bar{p}p \to p\bar{p}\pi^+\pi^-$	1.34 ± 0.10
	$p\bar{p}K^+K^-$	0.045 ± 0.016
	$p\bar{p}p\bar{p}$	≤ 0.03
6	$\bar{p}p \to p\bar{p}2\pi^+2\pi^-$	0.44 ± 0.06
	$p\bar{p}K^+K^-\pi^+\pi^-$	0.023 ± 0.012
	$2p2\bar{p}\pi^+\pi^-$	0.016 ± 0.010
8	$p\bar{p} \to p\bar{p}3\pi^+3\pi^-$	0.14 ± 0.04
	$4\pi^+4\pi^-$	0.015 ± 0.010
10	$p\bar{p} \to p\bar{p}4\pi^+4\pi^-$	0.04 ± 0.02
	$5\pi^+5\pi^-$	≤ 0.03

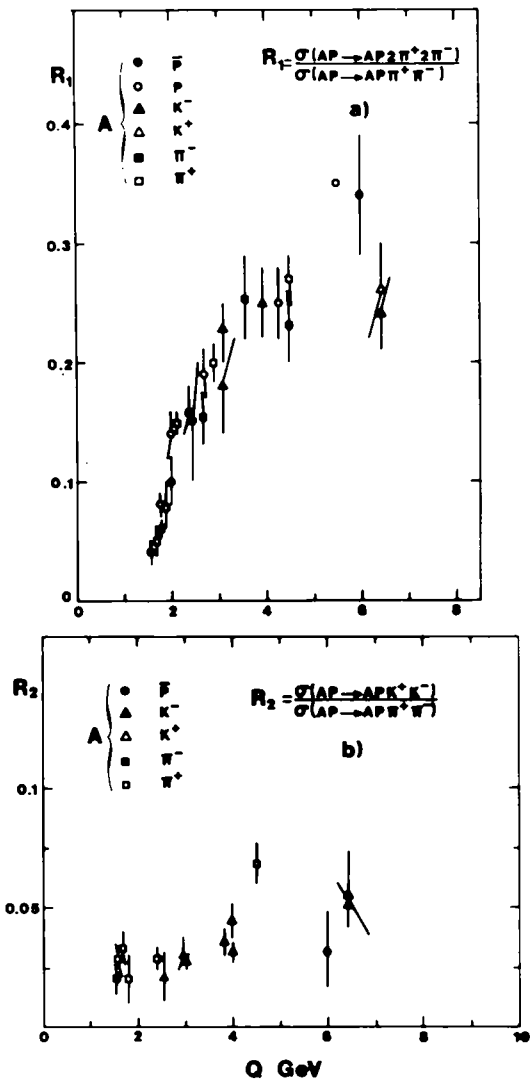

Fig. 11. Variation of the ratios R_1 and R_2 with the Q values of various 4-body and 6-body reactions.

the $s^{-0.47\pm0.07}$ energy dependence observed between 3.6 and 12 GeV/c [11] (fig. 12).

The main features of the reaction are best seen on fig. 13 where the c.m. rapidity of the π^- is plotted against the c.m. rapidity of the π^+. The sectors where the two rapidities have the same sign and the one corresponding to $y^*_{\pi^+} < 0$ and $y^*_{\pi^-} > 0$ are almost equally populated while the remaining one is practically empty. The

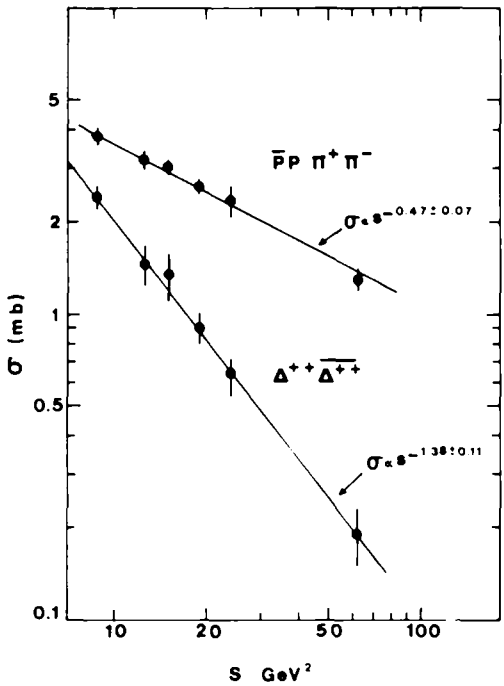

Fig. 12. Energy dependence of the total cross sections of the reactions $\bar{p}p \to \bar{p}p\pi^+\pi^-$, and $\bar{p}p \to \bar{\Delta}^{--}\Delta^{++}$.

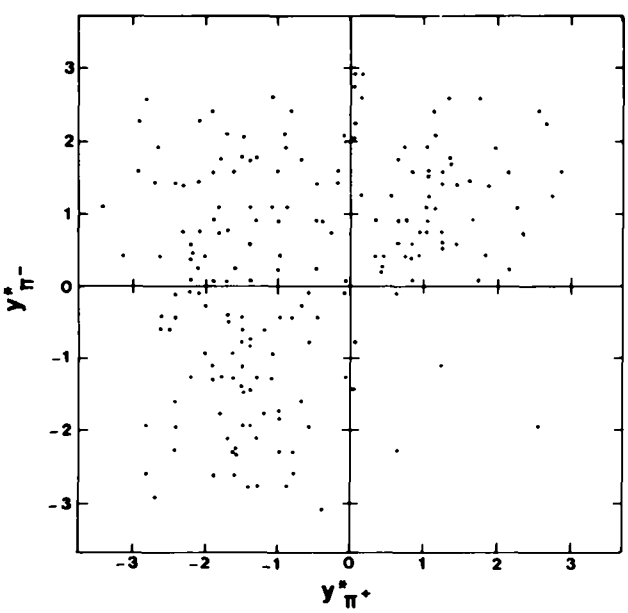

Fig. 13. Scatter plot of the $\bar{p}p\pi^+\pi^-$ events as a function of the c.m. rapidities of the two pions.

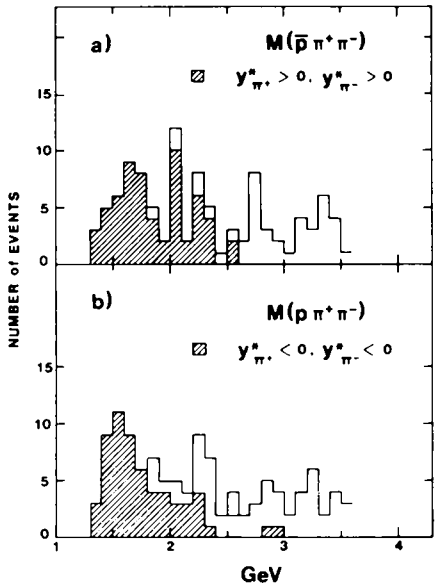

Fig. 14. (a) Distribution of $M(p\pi^+\pi^-)$ for all $\bar{p}p\pi^+\pi^-$ events and for those with $y^*_{\pi^+} > 0$ and $y^*_{\pi^-} > 0$; (b) Distribution of $M(p\pi^+\pi^-)$ for all $\bar{p}p\pi^+\pi^-$ events and for those with $y^*_{\pi^+} < 0$ and $y^*_{\pi^-} < 0$.

observed distribution is symmetric for reflection with respect to the diagonal $y^*_{\pi^+} = -y^*_{\pi^-}$ as required by C invariance.

The $p\pi^+\pi^-$ and $p\pi^+\pi^-$ mass distributions (fig. 14) show that the two sectors with $(y^*_{\pi^+} \cdot y^*_{\pi^-}) > 0$ correspond mainly to the diffractive dissociation of the target or the beam particle. The cross section for these diffractive processes is estimated

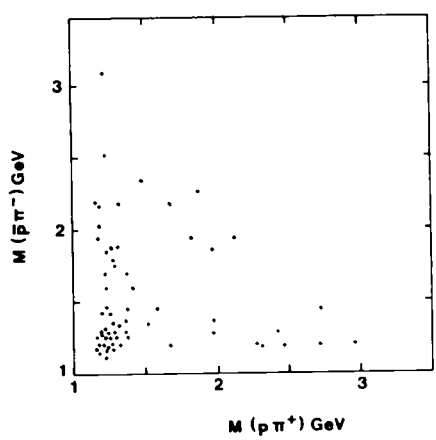

Fig. 15. Scatter plot of $M(\bar{p}\pi^-)$ *versus* $M(p\pi^+)$ for the $pp\pi^+\pi^-$ events with $y^*_{\pi^+} < 0$ and $y^*_{\pi^-} > 0$.

to 760 ± 40 μb for $M(p\pi\pi)$ or $M(\bar{p}\pi\pi)$ smaller than 2.5 GeV and thus corresponds to ~50% of the total cross section. In particular if we require $M(\bar{p}\pi\pi) < 2.2$.GeV, we obtain a cross section of 320 ± 30 μb for diffractive dissociation of the beam particle in agreement with the results obtained by the CERN-IHEP boson spectrometer at neighbouring energies (301 ± 12 and 277 ± 18 μb at 25 and 40 GeV/c respectively) [12].

The scatter plot of $M(\bar{p}\pi^-)$ versus $M(p\pi^+)$ for the events with $y^*_{\pi^+} < 0$ and $y^*_{\pi^-} > 0$ is presented in fig. 15. It is clearly seen that these events correspond mainly to the channel $\bar{p}p \to \bar{\Delta}^{--}\Delta^{++}$. The events falling in the area defined by $M(p\pi^+) < 1.4$ GeV and $M(\bar{p}\pi^-) < 1.4$ GeV correspond to a cross section of 190 ± 40 μb a value which can be taken as an estimate of the $pp \to \bar{\Delta}^{--}\Delta^{++}$ cross section. This result is in excellent agreement with the $s^{-1.38\pm0.11}$ energy dependence observed between 3 and 12 GeV/c [11] (fig. 12).

The ratio between the number of events which fall in the non-diffractive sectors $(y^*_{\pi^+} \cdot y^*_{\pi^-}) < 0$ of fig. 13 is equal to 10 ± 4, in good agreement with the value of 9 expected for $\bar{\Delta}^{--}\Delta^{++}$ and $\bar{\Delta}^0\Delta^0$ production by π exchange.

It is a pleasure to thank the operating crews of the Mirabelle bubble chamber, the IHEP accelerator and the RF beam as well as the scanning and measuring teams of the contributing laboratories.

References

[1] S.P. Denisov et al., Phys. Lett. 36B (71) 528.
[2] Y. Antipov et al., Nucl. Phys. B57 (73) 333.
[3] G. Akopdjanov et al., Nucl. Phys. B75 (74) 401.
[4] F. Grard et al., Phys. Lett., 59B (75) 409.
[5] D.B. Smith, Berkeley report, UCRL no. 20632 (1971); CERN-HERA 73-1.
[6] (a) J.M. Gramenitsky, Multiparticle production in $\bar{p}p$ interactions, Proc. Int. Conf. on high-energy physics, Tbilisi 1976, p. A2–3.
(b) Brussels-CERN-London-Mons-Orsay Collaboration, Inclusive V^0 production in $\bar{p}p$ interactions at 12 GeV/c, paper submitted to Tbilisi Conf., 1976.
(c) F.T. Dao et al., Phys. Lett. 51B (1974) 505 (14.75 GeV/c).
(d) D.R. Ward et al., Phys. Lett. 62B (1976) 237 (100 GeV/c).
(e) E.G. Boos et al., Nucl. Phys. B121 (1977) 381.
[7] (a) V. Blobel et al., Nucl. Phys. B69 (1974) 454 (12 and 24 GeV/c).
(b) V.V. Ammosov et al., Nucl. Phys. B115 (1976) 269 (69 GeV/c).
(c) M. Alston-Garnjost et al., Phys. Rev. Lett. 35 (1975) 142 (100 GeV/c).
(d) J.W. Chapman et al., Phys. Lett. 47B (1973) 465 (102 GeV/c).
[8] (a) R. Raja et al., Phys. Rev. D15 (1977) 627.
(b) J. Whitmore et al., Phys. Rev. Lett. 38 (1977) 996.
[9] (a) CERN-Hera 73-1 (p and $\bar{p}$);
CERN-Hera 70-4 (K^+);
CERN-Hera 70-6 (K^-);
CERN-Hera 72-1 ($\pi^\pm$).

(b) K^+p data:
G. Ciapetti et al., Nucl. Phys. B64 (1973) 58;
J.N. Carney et al., Phys. Lett. 55B (1975) 117;
D.C. Colley et al., Nucl. Phys. B50 (1972) 1;
P.L. Jain et al., Phys. Rev. D8 (1973) 738;
P. Davis et al., Nucl. Phys. B64 (1973) 58.
(c) K^-p data:
C. Louedec et al., Inclusive and exclusive cross sections in K^-p interactions at 14.3 GeV/c Saclay internal report, DPhPE 76-26, Nuovo Cimento, to be published.
[10] R. Barloutaud, Recent results on 32 GeV/c K^+p and $\bar{p}p$ interactions in the Mirabelle bubble chamber, Proc. Int. Conf. on high-energy physics, Tbilisi, 1976, p. A2-21.
[11] Ch. Walck et al., Nucl. Phys. B100 (1975) 61.
[12] Y.M. Antipov et al., Nucl. Phys. B99 (1975) 189.